Chemical Engineering Journal 180 (2012) 343–353

Contents lists available at SciVerse ScienceDirect

Chemical Engineering Journal

journal homepage: www.elsevier.com/locate/cej

Preparation, chemical and mechanical properties of microcomposite materials based on Fe powder and phenol-formaldehyde resin

M. Strečková [a,*], T. Sopčák [a], Ľ. Medvecký [a], R. Bureš [a], M. Fáberová [a], I. Batko [b], J. Briančin [c]

[a] Institute of Materials Research, Slovak Academy of Sciences, Watsonova 47, 043 53 Košice, Slovak Republic
[b] Institute of Experimental Physics, Slovak Academy of Sciences, Watsonova 47, 043 53 Košice, Slovak Republic
[c] Institute of Geotechnics, Slovak Academy of Sciences, Watsonova 45, 043 53 Košice, Slovak Republic

ARTICLE INFO

Article history:
Received 30 June 2011
Received in revised form 1 November 2011
Accepted 12 November 2011

Keywords:
Phenol-formaldehyde resin
Fe powder
Core–shell structure
Additives
Thermal degradation
Morphology

ABSTRACT

Preparation of microcomposite materials based on Fe powder and the modified phenol-formaldehyde resin (PFR) was investigated with the aim to design a new class of prospective soft magnetic materials. Undesirable evolution of water and other volatile by-products during curing process was eliminated by modification of resol prepolymer coating with two different inorganic additives – SiO_2 and $ZnSO_4$. The structure of synthesized PFR was confirmed by ^{13}C-NMR spectroscopy. The effect of both additives on thermal degradation, structure and morphology was studied by employing TG, DSC, IR and SEM analysis. The addition of $ZnSO_4$ into PFR caused a significant change in the polymer structure, which is constituted by nano-fibers linking Fe particles. The observed unusual structure of PFR–$ZnSO_4$ coating on Fe particles results in a higher mechanical hardness and flexural strength compared to the Fe particles coated by the pure PFR or PFR–SiO_2. It is shown that the microcomposites with a few percentages of PFR coatings exhibit a substantial increase of the specific resistivity and they still belong to soft magnetic materials with low enough coercivity.

1. Introduction

One of the most promising approaches in the preparation of nano- and microstructured composite materials is based on a modification of starting metal powders (Fe, Cu, Al and different metal alloys) through metallic [1–3], conductible [4] or insulating [5–7] non-metallic coatings. A particular scientific interest is concentrated on insulating polymers of different types, since metal-based composite materials with insulating spacer in between the metal particles ensures an interesting and rather specific electric and magnetic properties [8]. Bas et al. [9] divided soft magnetic composites (to be further abbreviated as SMC) into two categories. The first generation powder metallurgy (PM) prepared SMC includes pure iron, binary alloys Fe–Si, Fe–P, Fe–Ni, Fe–Co, the stainless steel and they are mainly suitable for direct current (DC) applications. The second generation of PM prepared SMC are amorphous and nanocrystalline materials produced by mechanical alloying or rapid solidification by melt spinning of alloys of the type Fe–Si–B–M (M is transition metal element). The resulting material of this kind has usually high magnetic induction, high resistivity and high permeability. The most highly developed materials from the second generation are insulated or encapsulated materials consisting of iron powder coated with a very thin, electrically insulating layer. These insulating materials have several advantages: magnetic properties are isotropic in the bulk, materials have smooth shape and enable a very efficient windings, which in turn give a higher thermal conductivity and permit a higher current input. The primary disadvantage is in their low mechanical strength, because they are not sintered. These ferromagnetic powder particles are used in many electromagnetic applications [10,11].

The preparation of composite materials with unique physical and mechanical properties can be achieved by combining well-known PM procedures with a chemical design of coated core–shell structures. The design of composite powder materials with desirable mechanical and physical–chemical properties is a very difficult task, because their chemical modification should simultaneously improve various properties such as density, dimensional and shape stability, tensile strength, electric, magnetic and optical properties, corrosion behaviour, etc. Moreover, the current effort is aimed at a rational design of applicable composite materials, which should also obey demanding environmental and economical requirements.

Phenol-formaldehyde (PFR) resins belong to the most useful substrates for the encapsulation of inorganic nanoparticles within polymeric networks [12]. These resins have been well known for over 100 years especially because of their low cost, aging endurance, dimensional stability and high-tensile strength

* Corresponding author. Tel.: +421 55 7922402, fax: +421 55 7922408.
E-mail address: mstreckova@imr.saske.sk (M. Strečková).

1385-8947/$ – see front matter © 2011 Elsevier B.V. All rights reserved.
doi:10.1016/j.cej.2011.11.036

[13,14]. PFR are known as the oldest thermosetting polymers and still have many industrial applications in different sectors such as automotive, computing, aeronautical and building industry. Final structural and mechanical properties of PFR depend on many factors involved in the synthesis of the prepolymer: temperature and time of condensation, pH, nature and amount of the catalyst, and initial formaldehyde to phenol molar ratio (F/P) [15].

The common PFR formed from phenol and formaldehyde in the alkali environment are extensively used in polymer composites and coating materials. Composites based on PFR, which contain inorganic particles, are particularly attractive because of higher thermal stability, decreased gas permeability, flame retardancy, improved mechanical and dimensional stability. Since resol-type resins have complex 3D structure prior to cure, intercalation is rather difficult [16]. This represents the most important limiting factor for the number of studies on these resins, compared to other thermosetting resins such as epoxy and unsaturated polyesters. Besides, the water formation as a by-product of cross-linking is also another problem of PFR. Namely, the properties of microcomposites are affected by the formation of micro voids, which occurs owing to the evaporation of initially existing water, other evolved gases [17] as well as the water formed as a by-product of the curing reaction [18]. The formation of microvoids can be partially eliminated applying a rather slow curing schedule however, this procedure does not completely resolve this problem.

The main goal of the present work was to prepare iron-based microcomposite materials where PFR coating was filled with two different inorganic additives SiO_2 and $ZnSO_4$. These materials were designed as a new class of dimensionally stable SMC with attracting combination of mechanical, electrical and magnetic properties. For this purpose, a lot of authors made considerable efforts to fulfill these requirements by incorporation of various reinforcing and filling constituents to polymer network. Typical fillers vary from silicas [19], exfoliated natural clays [20], carbon black [21] up to carbon nanotubes [22–24]. Three groups of phenolic matrix composites were investigated in the study of Wang et al. [25]: (1) phenolic resin filled by glass, ceramic and carbon black powder; (2) phenolic resin reinforced by graphite fiber; (3) phenolic resin reinforced by graphite fiber/glass powder. It has been demonstrated that the amount of voids was greatly reduced by introducing the glass powder to the phenolic resin. Among other matters, Wang et al. [25] proved that the composites reinforced by graphite fiber/glass particle exhibited higher flexural strength and flexural modulus than the phenolic composites reinforced by graphite fiber. The addition of a small amount of foreign nanoparticles (like clay or silica) significantly improves the engineering properties of the polymers (see Ref. [26] and references cited therein). Zhou et al. [27] reported a synthesis of high-performance thermoset composites using long fibers and nanoclays. The investigation of Suresha [28] shows that the improvement of polymer composites reinforced by filled fiber is generally determined by the interface attraction of filler, fiber, and polymer.

To the best of authors' knowledge, the design of microcomposite material, reinforced by polymeric fibers arising spontaneously during the preparation process has not been reported in the literature yet. This very unexpected and unusual uprise of polymeric fibers can lead to microstructures, which could be roughly compared with microstructures prepared by electrospinning methods [29–31].

To gain an insight into the very specific microstructure of prepared microcomposite materials, it was imperative to make a detailed analysis of PFR, PFR–SiO_2, PFR–$ZnSO_4$ using NMR and IR spectroscopy, DSC and TG methods in each step of the preparation process. Morphology and microstructure were examined in particular by employing SEM and EDX analysis. Last but not least, the mechanical strength, the flexural strength, the specific electrical resistivity and the magnetization process of the prepared microcomposites were also explored in detail.

2. Experimental

2.1. Materials and synthesis

The basic materials chosen for the preparation of microcomposites were iron powder (ASC 100.29 Höganäs) with size fraction in the range from 45 to 212 μm, dried SiO_2 and $ZnSO_4$ with average grain size around 150 nm. Phenol (99.0%, Aldrich), formaldehyde (37% aq, Aldrich), NH_3 (26% aq, Aldrich) were used for chemical synthesis of the pure PFR. Obtained chemicals were all analytical grade.

The initial reaction molar ratio of phenol/formaldehyde/ammonia (Ph/F/NH_3) was (1.0/1.5/0.35). The binary liquid mixture of phenol and formaldehyde was cooled in an ice bath and then the catalyst NH_3 (aq) was added dropwise. The result was white precipitate. The reaction mixture was refluxed for 1.5 h at 95 °C. Subsequently, water was removed under vacuum for 45 min at the same temperature. The final PFR was transparent with honey-like viscosity.

Two types of modified resins were prepared from PFR. The first was modified with SiO_2 and the second one with $ZnSO_4$. Both additives were firstly dried at 180 °C and then immediately added to the PFR in 40th min of water removing under vacuum. The resulting resins had the same character as pure PFR but they were a little bit cloudy due to addition of fillers. The composition of prepared samples and methods of their analyses and mechanical testing are listed in Table 1.

2.2. Coating and curing

The pure and modified resins were dissolved in acetone whereas the prepared solutions had water-like viscosity. The iron powder particles were added to those solutions. The suspensions were mechanically mixed in a beaker by the use of a glass rod. The iron particles coated with PFR, PFR–SiO_2 and PFR–$ZnSO_4$ were obtained in the form of the powder after a complete evaporation of the acetone from the suspension. A very fine white precipitate

Table 1
Composition of prepared samples and methods of characterization.

Samples	PFR (wt%)	Fe (wt%)	SiO_2 (wt%)	$ZnSO_4$ (wt%)	Methods
A	100	–	–	–	NMR, IR, TG, DSC
B	3	97	–	–	HV10, TRS, EDX
C	5	95	–	–	TG, HV10, TRS, EDX
D	90	–	10	–	IR, TG, DSC
E	90	–	–	10	IR, TG, DSC
F	4.5	95	0.5	–	TG, HV10, TRS, SEM, EDX
G	4.5	95	–	0.5	TG, HV10, TRS, SEM, EDX

Table 2
Curing schedule applied for each sample.

Temperature (°C)	40	60	80	90	100	110	120	130	150	180
Time (h)	24	24	8	1	16	0.5	1	1	0.5	0.25

was observed in the solution of PFR–$ZnSO_4$. The precipitate was extracted by 300 ml of acetone and dried on air for detailed IR analysis (described in Section 3.3). PFR–$ZnSO_4$ coating on Fe particles contained afore mentioned precipitate, which was mixed together with Fe powder during preparation of Fe–PFR–$ZnSO_4$ microcomposite. In order to prepare the final microcomposites Fe–PFR–SiO_2 and Fe–PFR–$ZnSO_4$, the coated powders were pressed into required shapes for mechanical testing at 800 MPa (see Section 2.6 for details on a shape and dimensions of prepared samples). Prepared samples were cured under ambient pressure according to the schedule described in Table 2.

2.3. Liquid ^{13}C NMR spectroscopy

Liquid ^{13}C NMR spectrum of uncured resins dissolved in DMSO was measured at ambient temperature using the Varian Mercury Plus 400 FT spectrometer with a ^{13}C frequency of 100.61 MHz. ^{13}C chemical shifts were measured with respect to tetramethylsilane (TMS) as the internal standard. The following measurement conditions were used: a pulse angle of 45°, a relaxation delay of 1.0 s, an acquisition time of 1.199 s, a spectral width of 25125.6 Hz and 5000 repetitions. DEPT spectrum was employed to separate the low intensity protonated carbons in the regions between 50 and 80 ppm.

2.4. IR spectra analysis

The chemical characterizations of PFR and the modified PFR with SiO_2 and $ZnSO_4$ additives were carried out by analysis of infrared spectra. The samples were prepared in the form of KBr pellets (1 mg sample + 300 mg KBr), analyzed using IR spectrophotometer (SPECORD M 80 Carl-Zeiss Jena) before and after curing.

2.5. Thermal analysis

Simultaneous DSC and TG analysis were performed by difference scanning calorimeter (METTLER 2000 C). The samples were heated up to 700 °C at a heating rate of 10 °C/min in an air atmosphere.

2.6. SEM, mechanical testing, specific resistivity and magnetic properties

The microstructure and morphology of prepared samples were observed by the scanning electron microscopy SEM (JEOL JSM-7000F) equipped with energy-dispersive X-ray spectroscopy EDX after carbon coating. Vickers hardness (test HV/10 was measured according to STN EN ISO 6507-1 (42 0374)), MPIF 43. For this purpose the samples were prepared in cylindrical shape of dimensions 10 mm × 3 mm ($d \times h$). The flexural strength (test according to standard STN 42 0891-4, MPIF 41) was measured on samples of prism shape 5 mm × 4 mm × 20 mm ($w \times h \times l$). The electrical resistivity was determined on the samples of prism shape with the same dimensions. Four probe AC measurements of electrical resistance at 100 Hz were performed using AC-current source and Lock-In Amplifier (SR 830). The magnetic measurement of the toroid-shaped samples with an outer diameter of 24 mm, inner diameter 17 mm and high of 2 mm were performed on the magnetometer based on the Faraday force balance method.

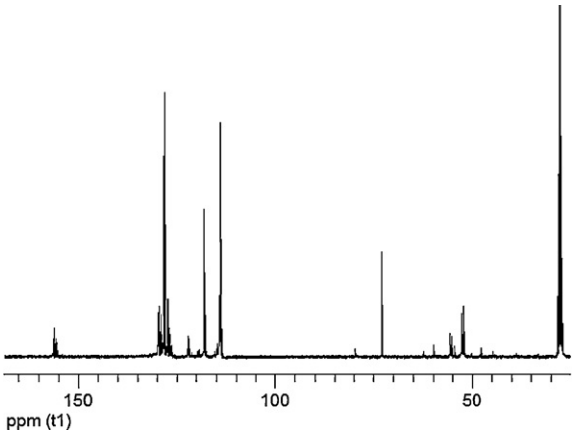

Fig. 1. ^{13}C NMR spectrum of sample A in DMSO.

3. Results and discussion

3.1. Liquid ^{13}C NMR analysis

First, let us look more closely at liquid ^{13}C NMR analysis, which will allow us to gain a deeper insight into the local chemical structure of the synthesized resin. Fig. 1 shows the ^{13}C NMR spectrum of synthesized pure resin. The chemical shifts adherent to certain functional groups observed in this spectrum are listed in Table 3. As shown in Fig. 1, there are number of signals which are characteristic for resol-type resins [32]. The signals with relatively low intensity in the region 157–155 ppm are typical for *ipso* carbons corresponding to phenol [33]. The signals in the range 130–126 ppm were assigned to substitute aromatic carbons in order *para*, *meta*, *ortho*. The region 118–114 ppm involves the signals from the unsubstituted *para* and *ortho* carbons. The signal at 73 ppm may be attributed to dimethylene ether bridges and the ones in the range 58–52 ppm belong to reactive methylol groups [34]. For illustration, the structure of resol-type resin discussed in above is schematically illustrated in Scheme 1. It should be noted that the chemical structure becomes more complicated during curing process on behalf of crosslinking.

3.2. Thermal analysis

TG and DSC thermograms of samples A, modified resole resins D, E and iron powders coated with pure and modified resin C, F and G are shown in Fig. 2a–c. Two significant regions, which occur during the heat treatment, can be observed in the TG and DSC records for the samples A, D, E shown in Fig. 2a and b. The first region from 125 to 225 °C relates to the polycondensation reaction

Table 3
Chemical shift assignment of phenol-formaldehyde resol resins in DMSO.

^{13}C NMR chemical shifts δ (ppm)	Group assignment
157–155	ipso carbons
130–126	Substituted aromatic carbons
118	Unsubstituted para carbons
114	Unsubstituted ortho carbons
73	Dimethylene ether bridges
52–58	Methylol groups
30–40	Methylene bridges

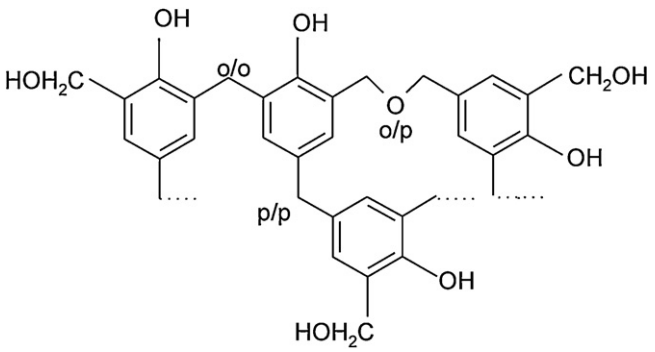

Scheme 1. A segment from the typical type of chemical structure of the resol resin [32].

and it is characterized by a mass loss with small exo-effect on DSC curves. The second region appears from 400 to 650 °C, where a gradual resin thermal degradation with corresponding mass losses and large exo-effects on DSC curves takes place. The main undesirable technological component released during the curing stage of resin (represented by the first region) is water [17]. To solve this problem we have used not only the prolonged heat treatment, but also SiO_2 and $ZnSO_4$ additives, which are assumed to be good water adsorbents. As it is clearly seen from the TG curves, the water evolution from the neat and modified resins with SiO_2 addition were significantly different (see Fig. 2a). The rapid evolution of water and other volatile by-products at 175 °C is evident in pure resin (sample A). Such a fast evaporation of gas products causes the formation of micro- and macrovoids in prepared resin and foaming at the surface of the Fe–PFR composites. Note that both additives contained some residuals of water (or crystalline water in $ZnSO_4$) despite of their drying at 180 °C (zoom in Fig. 2a). However, the substantially higher mass loss associated with the water release can be observed in the sample D (modified PFR with SiO_2 addition) up to 200 °C, which can be attributed to the higher amount of absorbed water due to the larger specific surface of SiO_2 compared to $ZnSO_4$. It is tempting to conjecture from Fig. 2a that a considerable amount of $ZnSO_4$ additive (as an ionic compound) was diluted into PFR (or into residual water of PFR) and it consequently changed the chemical structure of the resin. Fig. 2a indeed implies that the sample E with $ZnSO_4$ additive releases only slightly higher content of the adsorbed water than the sample A in contrast with the relevant behaviour of the sample D with SiO_2 additive. Moreover, the common trend in the TG curves of the samples D and E lies in a more gradual release of water and other gas products at lower temperature. This fact confirms an existence of some chemical interaction between both additives and the PFR resin.

In the case of the samples C, F and G one observes a small mass loss around 50 °C, which corresponds to release of chemically weakly bonded water (see Fig. 2c). Note furthermore that the highest mass loss up to 200 °C occurs in the iron powder coated with modified resin PFR–$ZnSO_4$ because of different interaction between

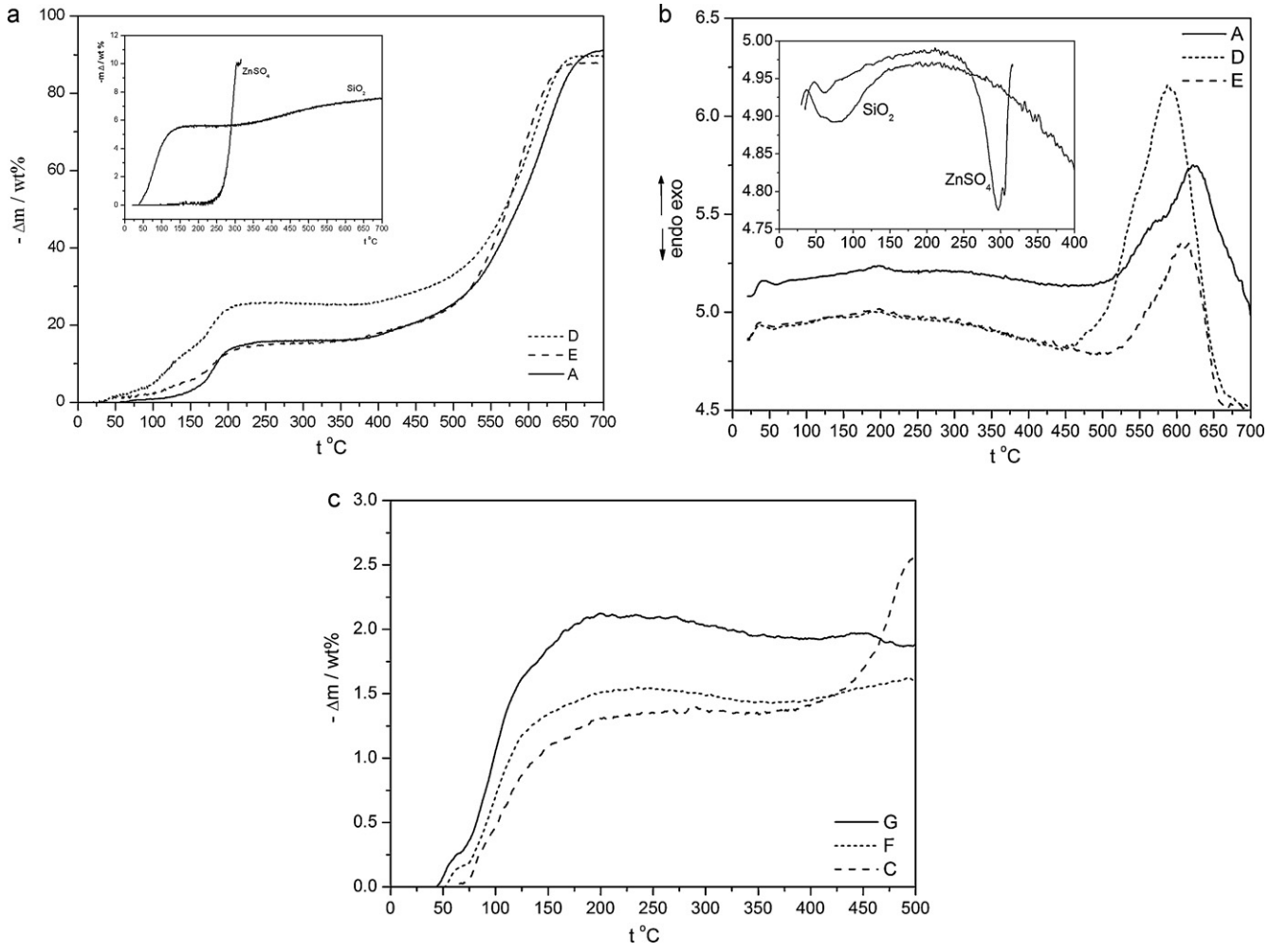

Fig. 2. (a) TG traces of the samples A, D and E; (b) DSC traces of the samples A, D and E; (c) TG traces of the samples C, F, G.

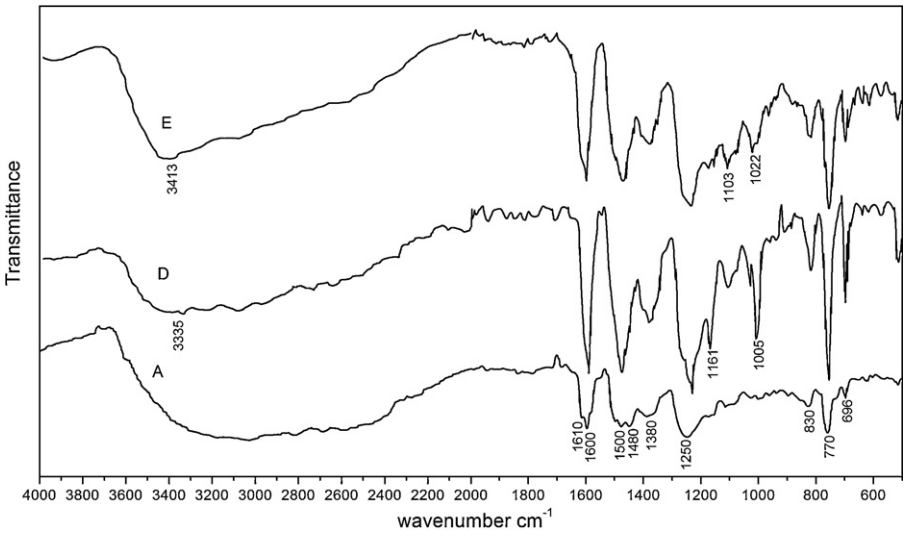

Fig. 3. IR spectra of non-cured samples A, D and E.

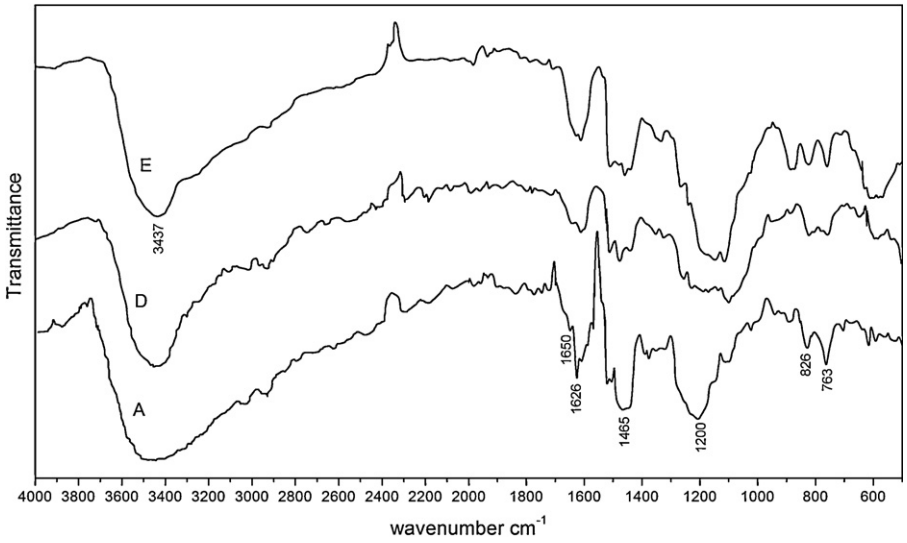

Fig. 4. IR spectra of cured samples A, D and E.

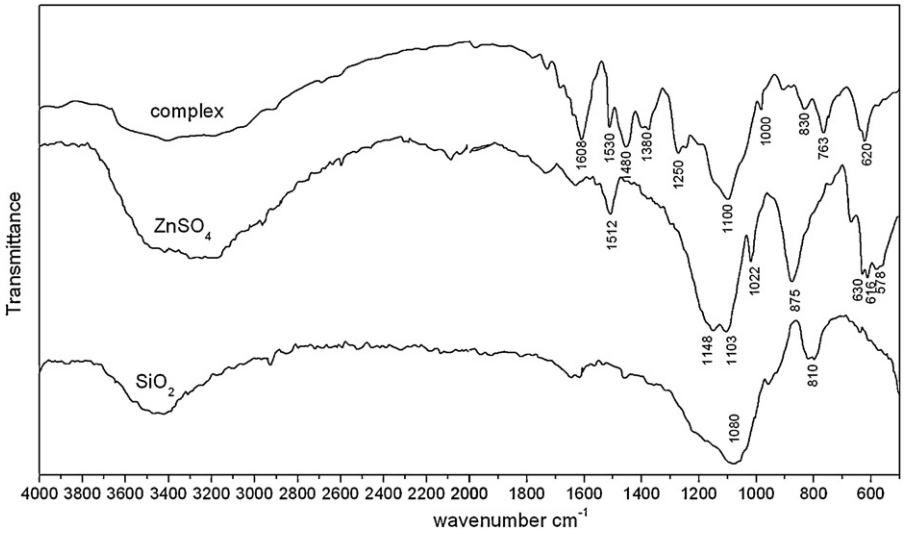

Fig. 5. IR spectra of SiO_2, $ZnSO_4$ and complex compound of PFR and $ZnSO_4$.

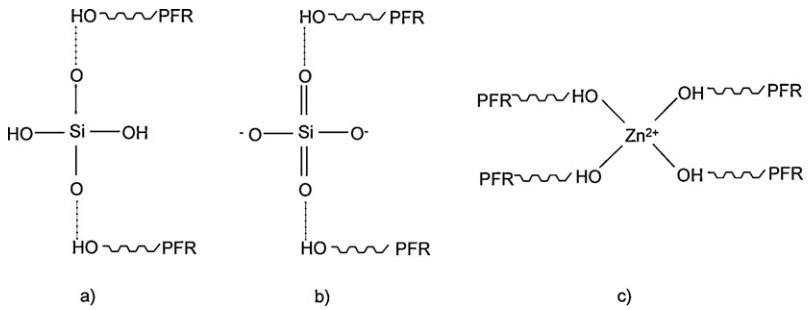

Scheme 2. Formation of hydrogen bonds between: (a) SiO_2 and PFR; (b) SO_4^{2-} and PFR; and the coordination bonds between: (c) Zn^{2+} and PFR.

Fe and both type of modified resins PFR–$ZnSO_4$ and PFR–SiO_2, respectively. It is quite evident that the interaction between Fe and PFR also substantially affects the crosslinking temperature of the resin in sample C, which is shifted toward lower temperature (around 100 °C) in comparison with the relevant crosslinking temperature (ca. 170 °C) of the sample A (Fig. 2a). It also turns out that the addition of SiO_2 or $ZnSO_4$ significantly enhances the thermal stability of modified resins in the samples F and G above 400 °C contrary to sample C.

3.3. IR spectra analysis

The IR spectra of uncured and cured samples A, D and E are shown in Figs. 3 and 4. Fig. 5 shows the IR spectra of pure additives SiO_2, $ZnSO_4$ and the complex of $ZnSO_4$ with PFR. The interpretation of major signals is summarized in Table 4.

The intense OH stretching vibrations form a broad peak (3000–3600 cm^{-1}), which reveals a presence of both phenolic as well as alcoholic groups [35] and residual of water. The maximum of OH aromatic stretching bands gradually shifts toward higher wavenumbers as a result of the effect of additives (Fig. 3) and this band becomes narrower owing to the crosslinking (Fig. 4). Besides, the band from plane vibrations of phenolic OH groups is clearly visible at 1380 cm^{-1} in the uncured samples (Fig. 3). Moreover, the creation of hydrogen bonds between resins and additives was estimated according to Scheme 2 illustrated below. The formation of hydrogen bonds support destabilization of phenolic OH groups and enhances the polymerization of resin. Narrowing of OH band is manifested after curing when the alcoholic OH groups decompose or oxidize to the carbonyl C=O group and subsequently, the novel peak appears at 1650 cm^{-1} in cured PFR (Fig. 4, the sample A). Due to the condensation reaction and crosslinking the band from C=C vibration are shifted to higher frequency (1626 cm^{-1}) and the intensity of CH_2 bridges (1450–1480 cm^{-1}) increases in the cured resin. The band at 1250 cm^{-1} in the uncured sample A can be attributed to the dimethylene ether bridges, which are more sensitive to alkalic condition and heat treatment than methylene bridges, and they decompose above 120 °C [36]. This indicates the broad peak at 1200 cm^{-1} in the sample A, which belongs to the alkyl-phenolic C–O stretch. A new absorption bands at 1161 cm^{-1} and 1005 cm^{-1} were found in the sample D and they were attributed to the interaction between PFR and SiO_2 (Fig. 3).

In the IR spectrum of pure SiO_2, the asymmetric stretching mode of the linear Si–O–Si was found at 1080 cm^{-1} and the bending mode

Table 4
Characteristic infrared absorption frequencies.

Band position (cm^{-1})	Assignments	Ref.
3600–3200	Phenolic, Alcoholic O–H stretch	[35]
3300–3100	Aromatic C–H stretch	[35]
2960–2850	Aliphatic C–H stretch	[35]
1650	Carbonyl C=O stretch	[35]
1626, 1610, 1600	Aromatic C=C ring stretch	[37,42]
1480, 1500	Aromatic C=C ring stretch	[42]
1380	OH in plane bend	[42]
1250	Biphenyl ether C–O stretch	[35,37]
1200	Alkyl-phenol C–O stretch	[38]
1148, 1103	Asymmetric ν_3 mode of SO_4^{-2}	[39]
1022	ν_1 mode of SO_4^{-2}	[39]
1080	Asymmetric Si–O–Si stretch	[40,41]
830, 770, 696	Out of plane substituted rings C–H deformation	[35]
810	Symmetric Si–O–Si stretch	[40,41]
630, 616, 578	Symmetric ν_4 mode of SO_4^{-2}	[39]

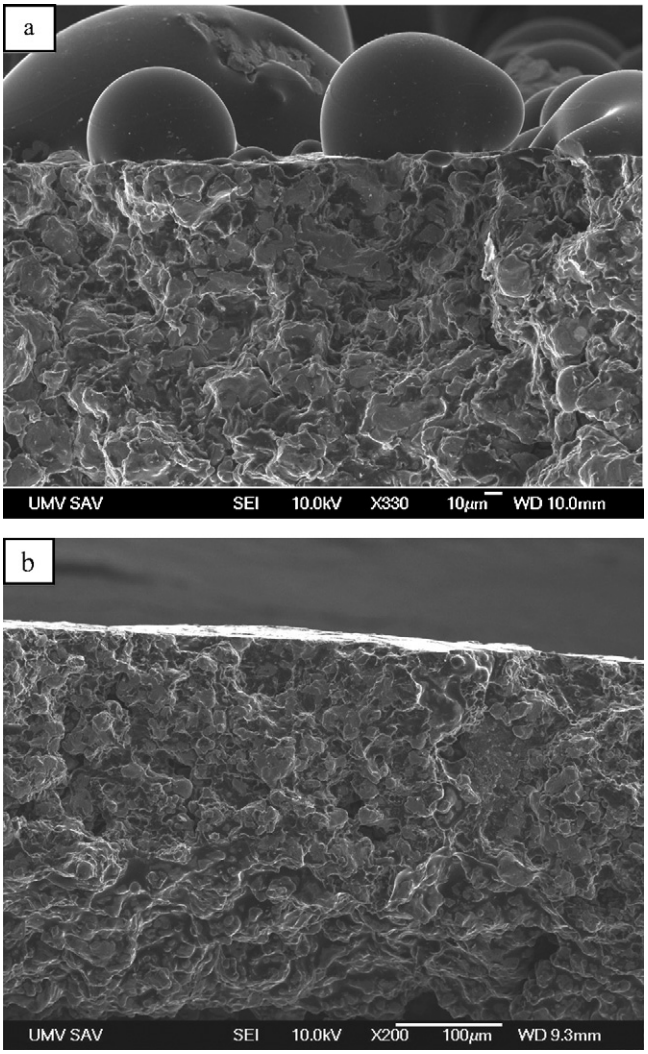

Fig. 6. (a) SEM image on macrostructure of (a) Fe–PFR without additives (negative effect of foaming), (b) Fe–PFR with SiO_2 additive.

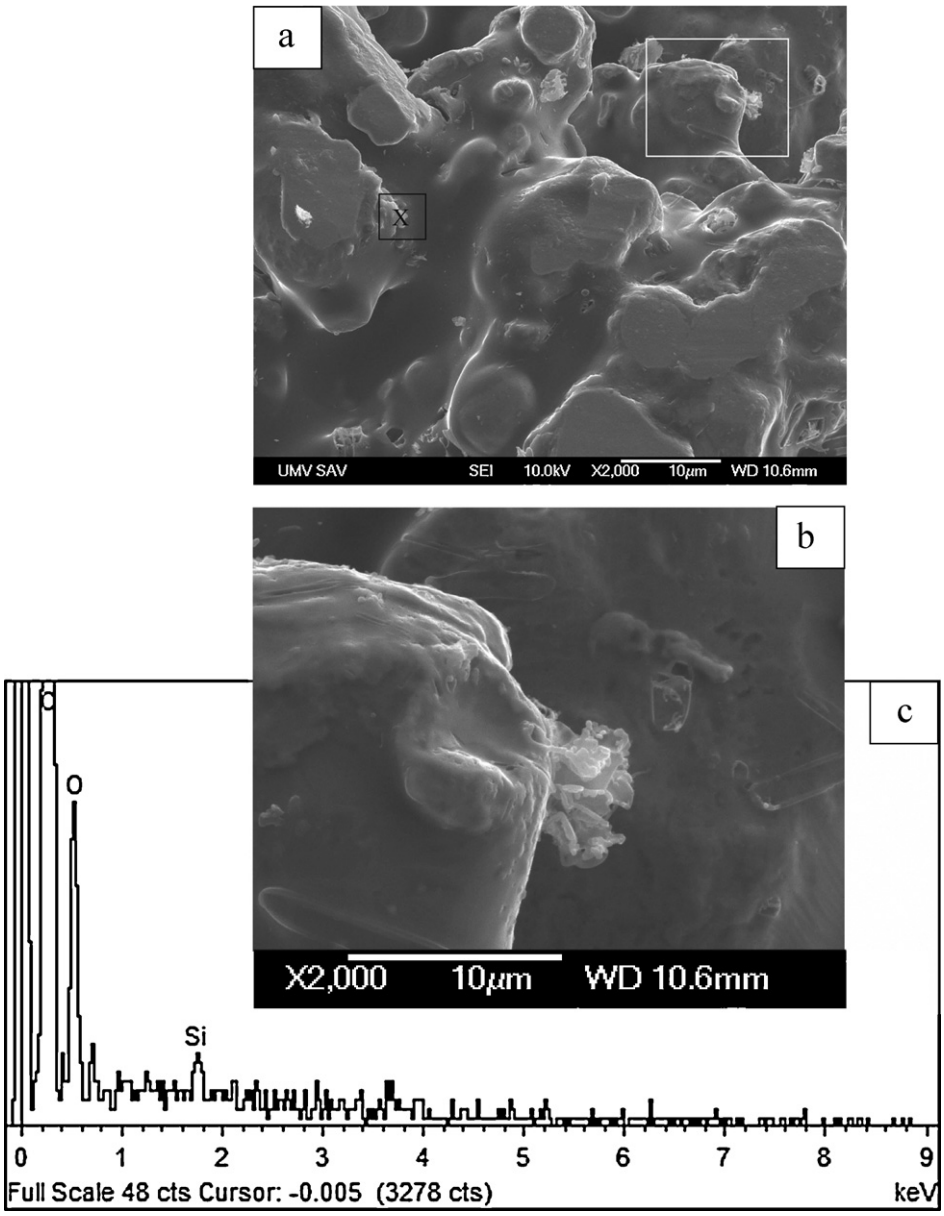

Fig. 7. (a) SEM micrographs of Fe–PFR–SiO_2 microcomposite before curing, (b) zoom on SiO_2 agglomerates sticked to PFR, (c) EDX analysis from place marked as x in (a).

of the O–Si–O bond was found at 810 cm^{-1} (Fig. 5). The IR spectrum of dried $ZnSO_4$ reveals two significant signals at 1148 cm^{-1} and 1103 cm^{-1}, which can be ascribed to the ν_3 mode of the SO_4^{2-}. Moreover, three additional peaks at 630, 616, and 578 cm^{-1} occur on behalf of the ν_4 mode of SO_4^{2-} anion (see Fig. 5). The signals at 1103 cm^{-1} and 1022 cm^{-1}, which correspond to SO_4^{2-} ions, can also be found in the IR spectrum of the sample E containing the uncured PFR–$ZnSO_4$ resin. The IR spectrum of the precipitate isolated after dilution of PFR–$ZnSO_4$ in acetone is presented in Fig. 5 (see the curve labeled as "complex"). The intensive SO_4^{2-} peak at 1100 cm^{-1} can be clearly seen in this spectrum. Besides, it is possible to observe here several peaks, which correspond to vibrations of specific groups of pure PFR (compare Fig. 5 with the spectrum of sample A in Fig. 3). One also finds from the detailed analysis of precipitate and the pure $ZnSO_4$ spectra the shift of this peak from 1148 to 1120 cm^{-1}, which reveals the formation of a complex between PFR and $ZnSO_4$ on behalf of hydrogen bonds and/or donor–acceptor bonds schematically illustrated in Scheme 2. The formation of complex compound PFR–$ZnSO_4$ thus arises due to a considerable versatility of Zn^{2+} and SO_4^{2-} ions to build coordination bonds with PFR.

3.4. Structural studies

The essential ingredient for the preparation of high-quality insulating composite materials is the knowledge of the chemical and phase composition of coating, its microstructure and interphase morphology, which depend on preparation conditions and basic properties of individual components. On the other hand, the structure and physical–chemical properties of prepared resin as well as mechanical properties of final-stage microcomposite materials can be basically influenced through the additives.

Fig. 6a and b implies that SiO_2 or $ZnSO_4$ addition has influence on the final shape and microstructure of composites after curing and both additives also act against surface deformation and PFR separation from the composite.

The different morphologies of modified PFR coating on Fe powder before curing are shown in Figs. 7 and 8. A very smooth and

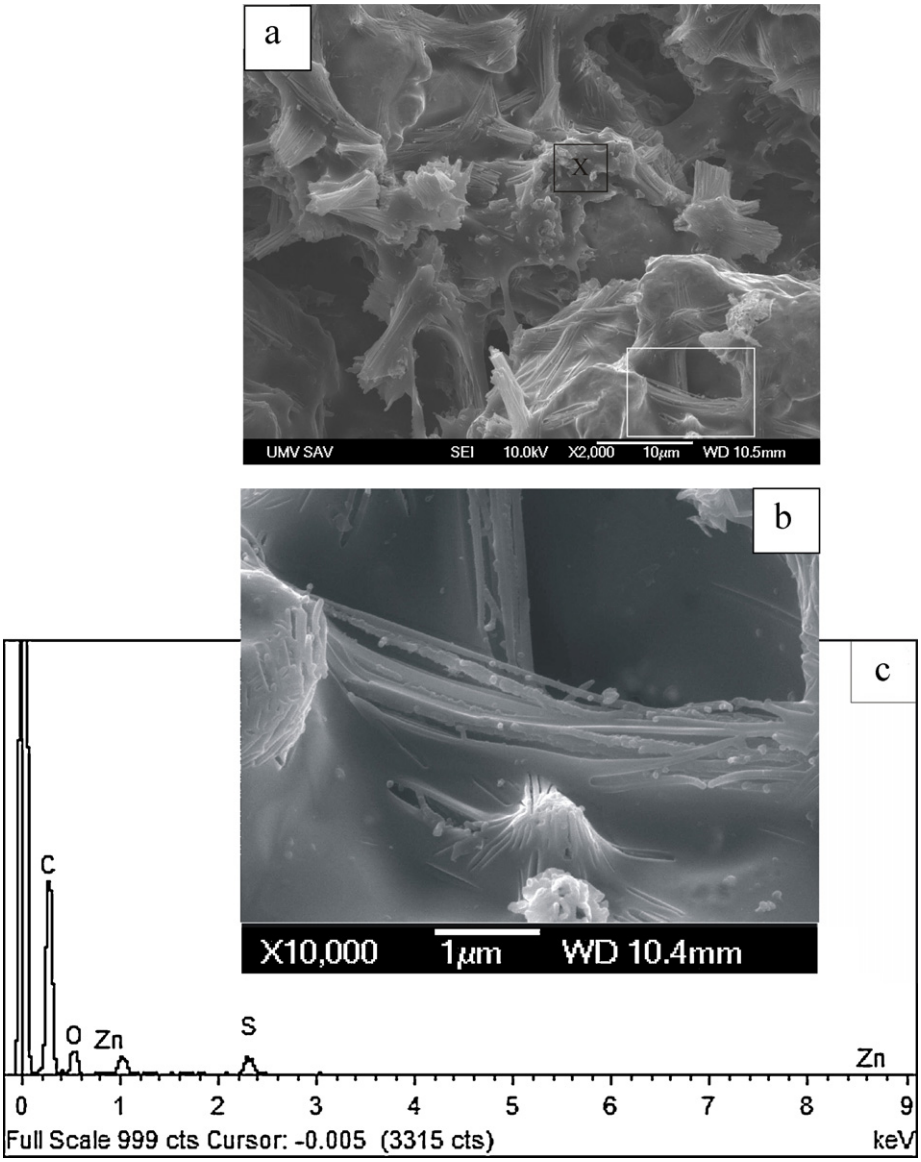

Fig. 8. (a) SEM micrographs of Fe–PFR–$ZnSO_4$ microcomposite before curing, (b) zoom on PFR fibers, (c) EDX analysis from place marked as x in (a).

uniform PFR–SiO_2 coating in the sample F with insertion of silica particles inside the resin is presented in Fig. 7a and b. Native SiO_2 agglomerates were confirmed in the coating by the EDX analysis (Fig. 7c) analysis from place marked as x in Fig. 7a. SiO_2 agglomerates with size around 1 μm are composed of fine 100 nm nanoparticles and they did not disaggregated during the composite preparation.

The very different morphology was observed in uncured PFR–$ZnSO_4$ coating (the sample G). It is evident from Fig. 8a that the addition $ZnSO_4$ provokes the polymerization of resin in to the form of fibers (Fig. 8b), which are spatially spread to all sides around Fe particles. To the best of authors' knowledge, the natural polymerization of resin into the fibrillar structure of this kind has not been reported in the literature yet. It is well known, however, that metal complexes are powerful initiators of homopolymerization of epoxy resins [43,44] and hence, one can suppose that creation of precipitate in the form of PFR–$ZnSO_4$ complex (as described in Section 3.3) could be the initial step for very specific polymerization resulting into the fibrillar structure. PFR fibers are approximately 10 μm long with thickness about 100 nm and the very small $ZnSO_4$ particles are located on their surfaces. Similarly as in the case of PFR–SiO_2 coating, some degree of $ZnSO_4$ particle agglomeration can be found in PFR–$ZnSO_4$ coating too. The incorporation of $ZnSO_4$ to the PFR structure was confirmed by EDX analysis (Fig. 8c).

The starting morphology of coatings consequently affects morphology of PFR coating after curing as it can be seen from Fig. 9a and b. The homogeneous, smooth and nonporous PFR–SiO_2 coating is apparent from Fig. 9a in contrast with PFR–$ZnSO_4$ coating (Fig. 9b), where a more rough but still compact coating is formed. The different morphology of PFR–$ZnSO_4$ coating arises because of the breakdown of PFR fibers during polymer melting at curing temperature, their contraction by surface tension to form of small drops with lower Gibbs free surface energy. No differences between microstructures of edged and polished sample B (Fe–PFR) and F, G were found. It can be seen in Fig. 10a and b that PFR creates macroscopically continuous phase around Fe particles, which verifies the uniform networking. The resin clusters are occasionally evident, but particles are tightly bonded and coated by PFR, without any visible coating exfoliation (Fig. 10b). The overall microstructure exhibits insignificant porosity, whereas the size of mostly irregular pores does not exceed 10 μm.

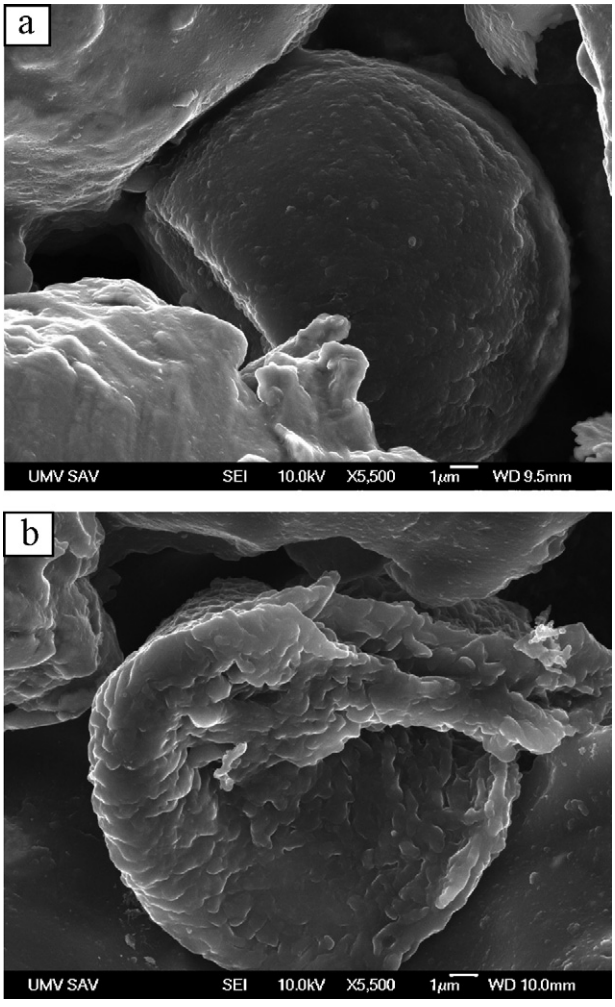

Fig. 9. SEM micrographs of (a) Fe–PFR–SiO_2 microcomposite after curing (b) Fe–PFR–$ZnSO_4$ microcomposite after curing.

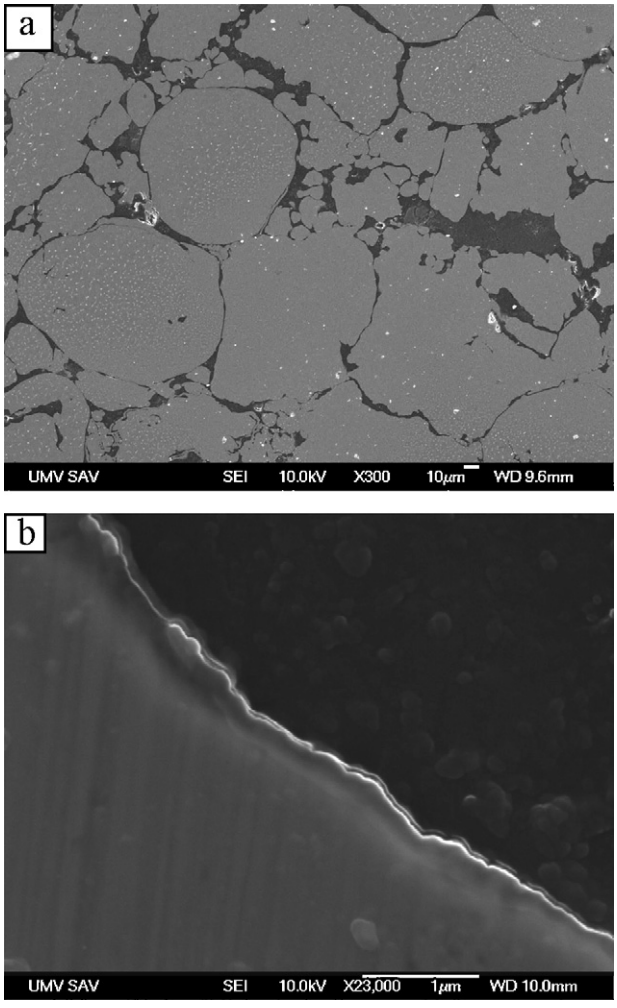

Fig. 10. SEM image on microstructrue of: (a) Fe–PFR microcompostite, (b) detail on PFR coating.

3.5. Mechanical, electric and magnetic properties

The substantial differences between the prepared microcomposite materials can also be found in their respective mechanical, electric and magnetic properties. The hardness of the pure commercial Fe sample sintered at 1100 °C and prepared by using the standard PM method is slightly higher than the hardness of the samples B and C without any additive (see Table 5). It is worthwhile to remark, moreover that the composite with $ZnSO_4$ additive (the sample G) shows much higher hardness than the pure Fe sample, at the expense of the flexural strength, which is however lowered just by few tens of percent. The effect of additives incorporated into the PFR coating is also evident from the measurement of electric resistivity. The growth of resistivity in the samples B and C evidently comes from the higher amount of electroinsulating component. The highest resistivity in the sample F can be attributed with a high certainty to incorporation of chemically inert SiO_2 fine particles into the PFR coating, which consequently prevents local contacts between Fe particles.

Finally, let us turn our attention to a preliminary study of magnetic properties of the prepared microcomposite materials. For illustration, Fig. 11a and b display the recorded hysteresis curves of the samples C and G in the DC applied magnetic field. Note furthermore that the other designed samples exhibit a very similar magnetization process and hence, let us merely quote in Table 5 their basic magnetic properties such as the coercive field and saturation induction. It can be easily understood from Table 5 that the prepared microcomposite materials indeed belong to the family of soft magnetic materials based on iron powder particles [45,46] with

Table 5
Mechanical, electric and magnetic properties of prepared microcomposites.

Sample	Hardness HV/10	Flexural strength (MPa)	Specific resistivity ρ (μΩ m)	Coercitive Field H_c (kA/m)	Saturation Induction B_{max} (T)
Höganäs Fe	115 [47]	–[a]	1.62×10^{-1}	0.12–0.2 [48]	1.0/1.3 [48]
B	93.26 ± 3.12	74.32 ± 3.61	3.16×10^{3}	0.19	1.2–1.3
C	83.63 ± 7.35	86.34 ± 5.88	4.58×10^{4}	0.26	1.1–1.25
F	112.37 ± 16.66	81.57 ± 16.01	2.42×10^{5}	0.34	1.1–1.25
G	200.67 ± 7.52	63.86 ± 10.19	1.03×10^{4}	0.29	1.15–1.25

[a] Not quoted due to a high plasticity of the sintered Fe.

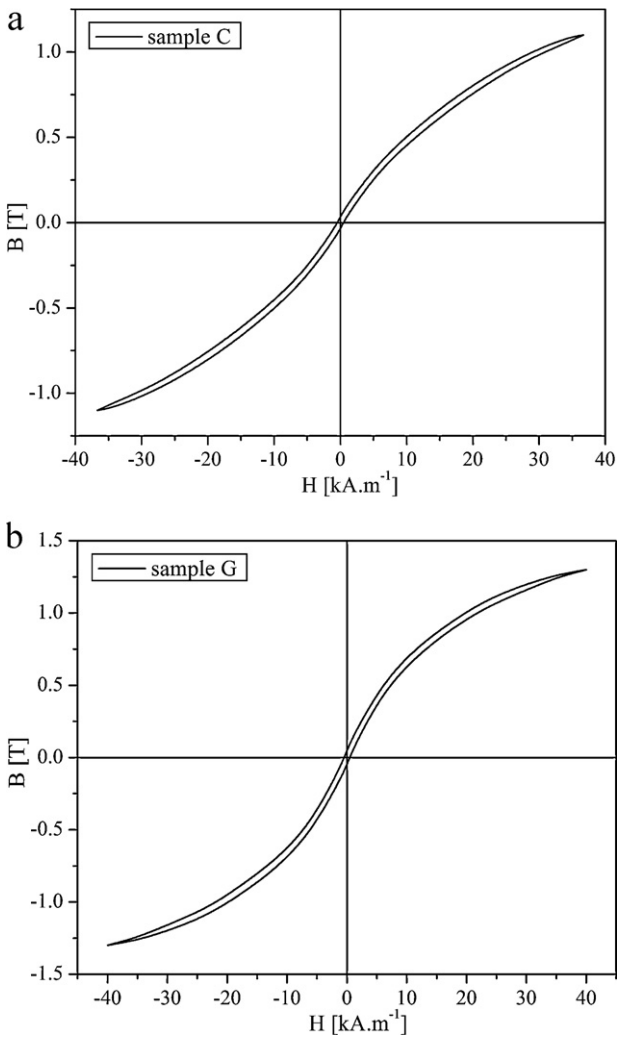

Fig. 11. DC hysteresis loops of: (a) sample C (b) sample G.

the coercive force in the range 0.19–0.34 kA/m and the saturation induction 1.1–1.3 T. The more detailed study of magnetic properties including the analysis of permeability, remnant induction, as well as the B–H loops and eddy current losses in AC magnetic field of different frequencies is left for our future work. It can be concluded however that the rather interesting combination of a high enough mechanical hardness and specific resistivity with sufficiently low coercive force of the designed SMC enables one to tailor a new prospective class of soft magnetic materials with several possible high-frequency applications.

4. Conclusions

The pure and modified PFR have been used for the preparation of a suitable insulation coating on the Fe powder microparticles, which were subsequently employed for a targeted design of prospective soft magnetic composites. The samples B and C with the pure PFR coating exhibit insufficient shape and dimensional stability due to the observed foaming on their surface, which is closely related to a release of water and other volatile gas products. This undesirable effect has been substantially suppressed by modifying PFR coating with two different inorganic additives SiO_2 and $ZnSO_4$. The addition of SiO_2 results in a more sufficient absorption of water, because this additive acts within the Fe–PFR–SiO_2 composite as inert filler homogenously distributed among the PFR. On the other hand, the addition of $ZnSO_4$ basically modifies the overall structure of Fe–PFR–$ZnSO_4$ composite by linking Fe powder through very fine fibers and it also works as a good water adsorbent. The observed fibrillar structure of Fe–PFR–$ZnSO_4$ microcomposite is also responsible for a substantial improvement of the mechanical hardness, which is even superior over the mechanical hardness of the pure sintered Fe. In addition, it turns out that the pure as well as modified PFR coatings form an excellent insulating spacer in between the Fe microparticles, which consequently leads to an enormous increase of the specific resistivity. The preliminary study of the magnetization process has confirmed that the prepared microcomposites belong to soft magnetic materials with a sufficiently low coercivity. The interestingly high mechanical hardness and specific resistivity in combination with low enough coercivity force implies several possible high-frequency applications of the prepared microcomposites owing to presumably small hysteresis and eddy-current losses. The more detailed study of magnetic properties in AC magnetic field will be subject of our further investigation.

Acknowledgements

We are thankful to both referees for useful comments and suggestions. This work was financially supported by the Slovak Grant Agency VEGA 2/0149/09 and Slovak Research and Development Agency under the contract no. APVV 0222/10.

References

[1] J.M. Castanho, M. Matos, M.T. Vieira, Reinforcement coating on stainless steel and copper powders, Microsc. Microanal. 14 (2008) 43–46.
[2] T.W. Clyne, Concise Encyclopedia of Composite Materials, second ed., Lausanne by Andreas Mortensen, Switzerland, 2007.
[3] A. Turoňová, M. Gálová, M. Šupicová, Parameters influencing the electrodeposition of a Ni–Cu coating on Fe powders. II. Effect of particle size fraction, suspension density and rotation speed, J. Solid State Electrochem. 7 (2003) 684–688.
[4] A. Oriňák, R. Oriňáková, A. Heile, I. Talian, M. Terhorst, H.F. Arlinghaus, Characterization of poly(methyl methacrylate) film deposited on iron powder particles by electropolymerization, Surf. Sci. 601 (2007) 4158–4162.
[5] S. Nakahara, E.A. Perigo, Y. Pittini-Yamada, Y. de Hazan, T.J. Graule, Electric insulation of a FeSiBC soft magnetic amorphous powder by a wet chemical method: identification of the oxide layer and its thickness control, Acta Mater. 58 (2010) 5695–5703.
[6] H. Shokrollahi, K. Janghorban, F. Mazaleyrat, M. Lo Bue, V. Ji, A. Tcharkhtchi, Investigation of magnetic properties, residual stress and densification in compacted iron powder specimens coated with polyepoxy, Mater. Chem. Phys. 114 (2009) 588–594.
[7] H. Brunckova, M. Kabátová, E. Dudrová, The effect of iron phosphate, alumina and silica coatings on the morphology of carbonyl iron particles, Surf. Interface Anal. 42 (2010) 13–20.
[8] H. Shokrollahi, K. Janghorban, Soft magnetic composite materials (SMCs), J. Mater. Process. Technol. 189 (2007) 1–12.
[9] J.A. Bas, J.A. Calero, M.J. Dougan, J. Magn. Magn. Mater. 254 (2003) 391–398.
[10] E. Bayramli, O. Olgelioglu, H.B. Ertan, Powder metal development for electrical motor applications, J. Mater. Process. Technol. 161 (2005) 83–88.
[11] L. Pennander, A.G. Jack, Soft Magnetic Iron Powder Materials AC Properties and their Application in Electrical Machines, paper presented at EURO Powder Metallurgy (EURO PM), Valencia, Spain, 2003.
[12] G.H. Padrón, F. Rojas, V. Castaño, Development and testing of anticorrosive SiO_2/phenolic-formaldehydic resin coatings, Surf. Coat. Technol. 201 (2006) 1207–1214.
[13] A. Gardziella, L.A. Pilato, A. Knop, Phenolic Resins, Springer-Verlag, Berlin Heidelberg, 2000.
[14] H. Sidney Goodman, Handbook of Thermoset Plastics, second ed., William Andrew, New Jersey, 1998.
[15] Y. Cohen, Z. Aizenshtat, Investigation of pyrolytically produced condensates of phenol-formaldehyde resins, in relation to their structure and decomposition mechanism, J. Anal. Appl. Pyrolysis 22 (1992) 153–178.
[16] C. Kaynak, C. Cem Tasan, Effects of production parameters on the structure of resol type phenolic resin/layered silicate nanocomposites, Eur. Polym. J. 42 (2006) 1908–1921.
[17] C. Chang, J.R. Tackett, Characterisation of phenolic resins with thermogravimetry-mass spectrometry, Termochim. Acta 192 (1991) 181–190.
[18] J. Wolfrum, G.W. Ehrenstein, Interdependence between the curing, structure and the mechanical properties of phenolic resins, J. Appl. Polym. Sci. 74 (1999) 3173–3185.

[19] Q.W. Yuan, J.E. Mark, Reinforcement of poly(dimethylsiloxane) networks by blended and in situ generated silica fillers having various sizes, size distributions, and modified surfaces, Macromol. Chem. Phys. 200 (1999) 206–220.
[20] R. Sengupta, S. Chakraborty, S. Bandyopadhyay, S. Dasgupta, R. Mukhopadhyay, K. Auddy, A short review on rubber/clay nanocomposites with emphasis on mechanical properties, Polym. Eng. Sci. 47 (2007) 1956–1974.
[21] S.H. Park, P.R. Bandaru, Improved mechanical properties of carbon nanotube/polymer composites through the use of carboxyl-epoxide functional group linkages, Polymer 51 (2010) 5071–5077.
[22] O. Breuer, U. Sundararaj, Big return from small fibers: a review of polymer/carbon nanotube composites, Polym. Compos. 25 (2004) 630–645.
[23] S.V. Ahir, Y.Y. Huang, E.M. Terentjev, Polymers with aligned carbon nanotubes: active composite materials, Polymer 49 (2008) 3841–3854.
[24] J.N. Coleman, U. Khan, W.J. Blau, Y.K. Gun'ko, Small but strong: a review of the mechanical properties of carbon nanotube polymer composites, Carbon 44 (2006) 1624–1652.
[25] S. Wang, S. Adanur, Bor Z. Jang, Mechanical and termomechanical failure mechanism analysis of fiber/filler reinforced phenolic matrix composites, Compos. Part B 28 (1997) 215–231.
[26] D. Lingaraju, K. Ramji, N.B.R. Mohan Rao, U. Rajya lakshmi, Characterization and prediction of some engineering properties of polymer – clay/silica hybrid nanocomposites through ANN and regression models, Proc. Eng. 10 (2011) 9–18.
[27] G. Zhou, S. Movva, J. Lee, Nanoclay and long-fiber-reinforced composites based on epoxy and phenolic resins, J. Appl. Polym. Sci. 108 (2008) 3720–3726.
[28] B. Suresha, G. Chandramohan, P.R. Sadananda Rao, P. Sampathkumaran, S. Seetharamu, Influence of SiC filler on mechanical and tribological behavior of glass fabric reinforced epoxy composite systems, J. Reinf. Plast. Compos. 26 (2007) 565–580.
[29] W.-E. Teo, S. Ramakrishna, Electrospun nanofibers as a platform for multifunctional, hierarchically organized nanocomposite, Compos. Sci. Technol. 69 (2009) 1804–1817.
[30] G.M. Bayley, M. Hedenqvist, P.E. Mallon, Large strain and toughness enhancement of poly(dimethyl siloxane) composite films filled with electrospun polyacrylonitrile-graft-poly(dimethyl siloxane) fibres and multi-walled carbon nanotubes, Polymer 52 (2011) 4061–4072.
[31] M.X. Wang, Z.H. Huang, F. Kang, K. Liang, Porous carbon nanofibers with narrow pore size distribution from electrospun phenolic resins, Mater. Lett. 65 (2011) 1875–1877.
[32] R. Rego, P.J. Adriaensens, R.A. Carleer, J.M. Gelan, Fully quantitative carbon-^{13}NMR characterization of resol phenol-formaldehyde prepolymer resins, Polymer 45 (2004) 33–38.
[33] G.A. Aierbe, J.M. Echeverrıa, I. Mondragon, Kinetics of phenolic resol resin formation by HPLC. III: zinc acetate, Polymer 40 (1999) 5873–5878.
[34] G. He, N. Yan, ^{13}C NMR study on structure, composition and curing behavior of phenol–urea–formaldehyde resole resins, Polymer 45 (2004) 6813–6822.
[35] Y. Chen, Z. Chen, S. Xiao, H. Liu, A novel thermal degradation mechanism of phenol-formaldehyde type resins, Termochim. Acta 476 (2008) 39–43.
[36] M.F. Grenier-Loustalot, G. Raffin, B. Salino, O. Paısse, Phenolic resins Part 6. Identifications of volatile organic molecules during thermal treatment of neat resols and resol filled with glass fibers, Polymer 41 (2000) 7123–7132.
[37] M. Křístková, P. Filip, Z. Weiss, R. Peter, Influence of metals on the phenol-formaldehyde resin degradation in friction composites, Polym. Degrad. Stab. 84 (2004) 49–60.
[38] L. Costa, L. Rossi di Montelera, G. Camino, E.D. Weil, E.M. Pearce, Structure–charring relationship in phenol-formaldehyde type resins, Polym. Degrad. Stab. 56 (1997) 23–35.
[39] T. Nishida, K. Kawakami, Local structure of x K_2SO_4. $(95-x)$ $ZnSO_4{\cdot}5CoSO_4$ glassed and crystallization of $60K_2SO_4{\cdot}30ZnSO_4{\cdot}5CoSO_4{\cdot}5Fe_2(SO_4)_3$ glass, Solid State Commun. 107 (1998) 453–458.
[40] G.H. Padron, F. Rojas, M. Garcia-Garduno, M.A. Canseco, V.M. Castano, Development of hybrid materials of consisting of SiO_2 microparticles embedded in phenolic-formaldehydic resin polymer matrices, Mater. Sci. Eng. A 355 (2003) 338–347.
[41] T. Periadurai, C.T. Vijayakumar, M. Balasubramanian, Thermal decomposition and flame retardant behaviour of SiO_2–phenolic nanocomposite, J. Anal. Appl. Pyrolysis 89 (2010) 244–249.
[42] I. Poljansek, M. Krajnc, Characterization of phenol-formaldehyde prepolymer resins by in line FT-IR spectroscopy, Acta Chim. Slov. 52 (2005) 238–244.
[43] M. Doring, U. Arnold, Polymerization of epoxy resins initiated by metal complexes, Polym. Int. 58 (2009) 976–988.
[44] K.F. Lin, W.Y. Shu, T.L. Wey, Organotransition metal complexes as additives for epoxy resins: 2. Interaction with epoxy resins, Polymer 34 (1993) 277–288.
[45] R. Boll, in: R.W. Cahn, et al. (Eds.), Materials Science and Technology, Wiley VCH Verlag, Weinheim, 1994, p. 401.
[46] K.H.J. Buschow, F.R. De Boer, Physics of Magnetism and Magnetic Materials, Kluwer Academic Publishers, New York, 2004, p. 155.
[47] Höganäs Corporation, Höganäs eisen-und stahlpulver fur sinterformteile 1998, pp. 79–83.
[48] K. Narasihman, F. Hanejko, M.L. Marucci, World Congress on Powder Metallurgy and Particulate Materials, 2008, Washington D.C.